Physics-based modeling of a bi-layer Al_2O_3/Nb_2O_5 analog memristive device

Richard Schroedter*, Eter Mgeladze†, Melanie Herzig†, Alon Ascoli*,
Stefan Slesazeck†, Thomas Mikolajick†‡, Ronald Tetzlaff*

*Chair of Fundamentals of Electrical Engineering, Technische Universität Dresden, Dresden, Germany
†NaMLab gGmbH, Dresden, Germany
‡Chair of Nanoelectronics, Technische Universität Dresden, Dresden, Germany

***Abstract*—This paper proposes the derivation of a physics-based model of an analog memristive device realized as a bi-layer Al_2O_3/Nb_2O_5 stack. Memristive crossbar arrays implementing matrix-vector multiplications are a central building block of novel computing-in-memory architectures for artificial neural network and neuromorphic computing applications. The presented memristor shows analog, multi-level switching at high resistances without electroforming and is suitable for crossbar operations with low energy consumption. By including a graphical analysis method of the I-V curves obtained in a quasi-static approach, the dynamic behavior is analyzed with regard to ohmic and Poole-Frenkel behavior. Finally, a compact model, represented by an algebraic differential equation, is proposed and verified by fitting calculated solutions to experimental data.**

***Index Terms*—Physics-based compact model, bi-layer Al2O3/Nb2O5 stack, analog memristive device, Poole-Frenkel emission, crossbar array for neuromorphic computing**

I. Introduction

Analog memristive devices are potential candidates for implementing brain-inspired computing, also known as neuromorphic computing, including artificial neural networks [1], [2]. Memristive crossbar arrays can perform computational intensive matrix-vector multiplications applying Kirchhoff's law for the weighted summation of currents with high energy efficiency [3], [4]. Various redox-based resistive switching memories have been studied in literature to fulfill the requirements for crossbar application [5], where nanodevices with two oxide layers can provide high nonlinearity while limiting the current through the device [6]–[9]. A metal-insulator-insulator-metal (MIIM) device with a bi-layer Al_2O_3/Nb_2O_5 stack was introduced in [10], [11], where the analog resistive switching is attributed to charge trapping and detrapping. This type of memristor has been integrated in a crossbar array, can be activated without electroforming and shows favorable multi-level switching behavior at high resistances of several MΩ [11]. Different from previously presented NbO memristors manufactured at NaMLab gGmbH [12], [13], the presented device does not feature negative differential resistance for the operating voltage range. Endurance with resistive switchings of more than 100 cycles with a switching speed in range of µs to ms have been demonstrated in [10], while state retention is within hours up to days [14]. The simulation of the memristive crossbar performance requires an appropriate compact modeling of the devices. The modeling also helps to understand and further optimize the device behavior.

We propose a physics-based modeling by applying a graphical analysis [15] of the measurements and using Poole-Frenkel emission as main conduction mechanism. Furthermore, the dynamic route map (DRM) [16] of the state equation, which is part of the proposed voltage-controlled extended memristor model, is analyzed.

The paper is organized as follows: Section II describes the fabrication of the memristor. Section III and IV present the modeling methodology, applying a graphical analysis resulting in a compact physics-based model in sec. V. The results are discussed in sec. VI with respect to the crossbar application and finally the conclusion is given in sec. VII.

II. Fabrication

The memristive bi-layer stacks were fabricated at NaMLab gGmbH on $2 \times 1\,\mathrm{cm}$ Si coupons with $1.5\,\mathrm{nm}$ SiO_2. For the MIIM stack processing following steps were carried out: firstly, $300\,\mathrm{nm}$ aluminum stripes were thermally evaporated for the secure contacting of the device after fabrication. A $20\,\mathrm{nm}$ Ti bottom electrode was deposited using DC magnetron sputtering which was followed by a reactive ion sputtering of $2\,\mathrm{nm}$ Al_2O_3 tunneling barrier, as illustrated in Fig. 2a. In order to process $10\,\mathrm{nm}$ of stoichiometric Nb_2O_5, metallic Nb target was DC sputtered at the constant pressure of $1.1 \times 10^{-3}\,\mathrm{mbar}$ and the mass flow ratio of Ar to O_2 of 0.67. Finally, circular top electrodes made of $30\,\mathrm{nm}$ Ti and $30\,\mathrm{nm}$ Pt were deposited by electron beam evaporation. The top electrodes were structured using a shadow mask where contact diameters were ranging from 20 to $100\,\mu\mathrm{m}$. All the processing steps were performed at room temperature. The X-Ray reflectometry and ellipsometer were used for the exact monitoring of metallic and oxide layer thickness. The electrical characterization was performed on a probe station using parameter analyzer (Keithley 4200, Tektronix Inc., US) at room temperature. On the MIIM stack the voltage was always applied to the top electrode (TE) and the bottom electrode (BE) was kept grounded.

This work was supported by the German Research Foundation (DFG) under the Project No. 441898364.

Post-print version of the article: R. Schroedter, E. Mgeladze, M. Herzig, A. Ascoli, S. Slesazeck, T. Mikolajick, R. Tetzlaff, "Physics-based modeling of a bi-layer Al2O3/Nb2O5 analog memristive device", *Proc. of the IEEE International Symposium on Circuits and Systems (ISCAS), 2022, Austin, TX, USA*, 2022. DOI: 10.1109/ISCAS48785.2022.9937966

For further information contact: richard.schroedter[at]tu-dresden.de, ORCID: 0000-0003-3259-4571

III. Graphical analysis

The memristor is characterized by quasi-static current-voltage (I-V) measurements with 10 mV steps shown Fig. 1a. First a negative voltage up to −4 V is applied to activate the device, which switches the resistance from several hundred MΩ down to the range of 5 up to 9 MΩ. The activation step shows a smooth I-V characteristic like interfacial switching, which is different to the electro-forming in filamentary switching devices [12]. Then, the device is reset with consecutive gradual voltage sweeps (cf. regions I to V in Fig. 4a). Solid (dashed) lines in Fig. 1a indicate increasing (decreasing) voltage sweeps for both the set and reset switching transitions. Afterwards a full sequence of set, reset and set operations with intermediate readings up to 1 V (cf. regions VI, VIII, X and XII for readings in Fig. 4a) are performed.

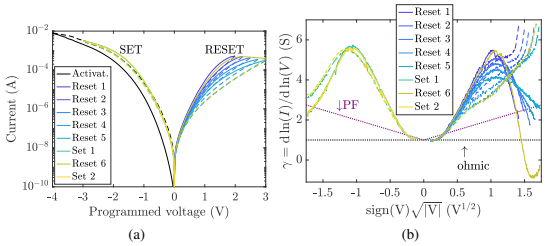

Fig. 1: I-V measurement: (a) First an activation step, then five gradual resets 1 to 5 up to [2.0, 2.25, 2.5, 2.75, 3.0] V (cf. regions I to V in Fig. 4a), followed by a set 1, full reset 6 and set 2 (cf. regions VII, IX and XI in Fig. 4a), readings not shown; (b) Exponential derivative $\gamma = \mathrm{d}\ln(I)/\mathrm{d}\ln(V)$ providing insights to equivalent circuit as demonstrated in [15]; Solid (dashed) lines are for increasing (decreasing) voltage. The dotted lines in (b) indicate the ideal behavior for ohmic and Poole-Frenkel (PF) emission.

To model the I-V characteristic the graphical analysis approach using exponential derivative proposed in [15] for memristors having Poole-Frenkel and Schottky emission is performed. This includes modeling of a nonlinear device with Poole-Frenkel or Schottky emission G_m with a parallel resistor R_p and a series resistor R_s as shown in Fig. 2b. The exponential derivative, shown in Fig. 1b,

$$\gamma = \frac{\mathrm{d}\ln(I)}{\mathrm{d}\ln(V)} \tag{1}$$

is calculated from the measurement of Fig. 1a. The dotted lines in Fig. 1b indicate the ideal behavior for ohmic and Poole-Frenkel emission. For the set as well as for the reset by looking at increasing voltages, this analysis provides similar curve shapes as proposed by [15] for nonlinear Poole-Frenkel conduction element in parallel with an ohmic resistance R_p and in series with a second resistance R_s. However, two clear differences to [15] can be observed in Fig. 1b: (i) while the increasing voltages (solid lines) follow a bow shape, the decreasing voltages (dashed lines) follow a more linear shape during reset and (ii) the reset 6 has negative γ values. Due to (i) the conduction mechanisms might be considered to be different

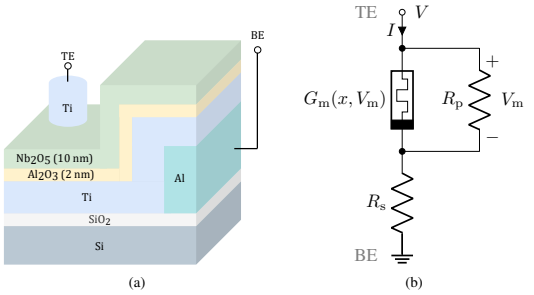

Fig. 2: Memristive device: (a) Fabricated stack and (b) equivalent circuit model

for set and reset. While (ii) is difficult to explain, it may indicate a strong voltage dependence of the trapped/detrapped charges.

IV. Physics-based modeling

For niobium oxide devices several conduction mechanism have been reported, like Poole-Frenkel emission [12], [13], [17], Schottky emission [6] and also Fowler-Nordheim tunneling through the aluminum oxide barrier [8], [18]. The interfacial analog switching due to trapping and detrapping of charges at the oxide interface of Al_2O_3/Nb_2O_5 is described in [10]. The derivative curves in Fig. 1b indicate ohmic behavior because γ starts near one for small voltages. We speculate that Poole-Frenkel (PF) emission occurs, which also starts for γ around one. The following inclination in Fig. 1b is assigned to the parallel and series resistance circuit as described in [15].

Fig. 3 shows plots of the measurement data according to the physical equations for ohmic conduction $I/V = 1/R_p$ and Poole-Frenkel emission with

$$\ln\left(\frac{J_\mathrm{PF}}{E}\right) = \frac{\sqrt{\frac{q^3}{\pi\varepsilon_0\varepsilon}}}{k_\mathrm{B}T}\sqrt{E} - \frac{q\phi_\mathrm{T}}{k_\mathrm{B}T} + \ln(q\mu N_\mathrm{C}) \tag{2}$$

relating the current density $J = I/A$ and the electrical field $E = V/d$, where is $A = \pi D^2/4$ the cross-sectional area of the top electrode with the diameter of $D = 50\,\mu\mathrm{m}$, d the

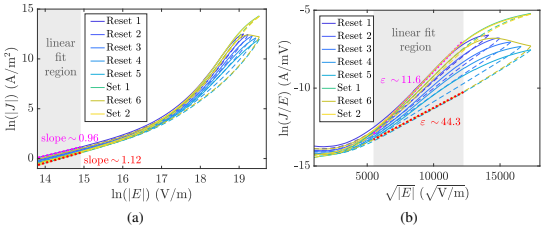

Fig. 3: Graphical analysis of the I-V behavior: (a) Double logarithmic plot to analyze ohmic with slope of linear fit for R_p and (b) Poole-Frenkel plot with ε from slope of linear fit. Solid/dashed lines indicate increasing/decreasing voltage. Linear fitting of the data is indicated for top and bottom line in the gray area plotted as thick dotted lines.

Post-print version of the article: R. Schroedter, E. Mgeladze, M. Herzig, A. Ascoli, S. Slesazeck, T. Mikolajick, R. Tetzlaff, "Physics-based modeling of a bi-layer Al2O3/Nb2O5 analog memristive device", *Proc. of the IEEE International Symposium on Circuits and Systems (ISCAS), 2022, Austin, TX, USA*, 2022. DOI: 10.1109/ISCAS48785.2022.9937966

For further information contact: richard.schroedter[at]tu-dresden.de, ORCID: 0000-0003-3259-4571

oxide thickness. In (2) q denotes the elementary charge, μ the electron mobility, N_C the density of states in the conduction band of the dielectric, ϕ_T the trap barrier height, $\varepsilon_0\varepsilon$ the dielectric permittivity, k_B the Boltzmann constant and T the ambient temperature of 25 °C if not noted otherwise.

Linear fitting for the ohmic conduction for voltages between 10 mV and 30 mV (cf. slopes in gray area in Fig. 3a are between 0.96 and 1.12) results in resistances R_p between 5 and 9 MΩ. Linear fitting using $\ln(J_\mathrm{PF}/E) = S_\mathrm{PF}\sqrt{E} - y_\mathrm{off}$ for the PF emission for voltages between 0.3 V and 1.5 V (gray area in Fig. 3b) results in permittivities ε between 11.6 and 44.3, calculated with $\varepsilon = q^3/\pi\varepsilon_0(k_\mathrm{B}TS_\mathrm{PF})^2$ by using the slope S_PF of the linear fit, which is in the range of reports from literature [19]. The normalized fit offset $y_\mathrm{off}/k_\mathrm{B}T$ which is referring to the trap barrier height varies only little between 0.40 eV and 0.45 eV. For voltages above 1.5 V we therefore assume the main effect by the memristor state change of charge trapping and detrapping in the following.

V. Compact physics-based state model

The memristor in the MIIM device is modeled as extended generic memristor with

$$I_\mathrm{m} = G_\mathrm{m}(x, V_\mathrm{m}) \cdot V_\mathrm{m}, \quad \text{and} \quad \frac{\mathrm{d}x}{\mathrm{d}t} = f(x, V_\mathrm{m}). \tag{3}$$

For the compact physics-based state model, the different effects need to be combined into one equation. Therefore we apply ohmic and Poole-Frenkel-like equations. The ohmic behavior is represented by the parallel resistor R_p, while the Poole-Frenkel behavior is represented by a nonlinear memristor $G_\mathrm{m}(x, V_\mathrm{m})$.

Assuming the equivalent circuit (cf. Fig. 2b) with a series resistor R_s and a parallel resistance R_p to a nonlinear memristive device $G_\mathrm{m}(x, V_\mathrm{m})$, the total current I and the MIIM voltage V and the memristor voltage V_m are given with

$$I = G_\mathrm{m}(x, V_\mathrm{m}) \cdot V_\mathrm{m} + \frac{V_\mathrm{m}}{R_\mathrm{p}}, \quad \text{and} \quad V_\mathrm{m} = V - IR_\mathrm{s}. \tag{4}$$

In agreement with the experimental data in Fig. 3b a Poole-Frenkel-like behavior is assumed [18]

$$G_\mathrm{PF}(V_\mathrm{m}) = \frac{q\mu N_\mathrm{C} A}{d} \exp\left(\frac{-q\left(\phi_\mathrm{T} - \sqrt{\frac{qV_\mathrm{m}}{\pi\varepsilon_0\varepsilon d}}\right)}{k_\mathrm{B}T}\right) \tag{5}$$

with a square root dependency on the memristor voltage V_m in the exponent

$$G_\mathrm{PF}(V_\mathrm{m}) = B\exp\left(C\sqrt{V_\mathrm{m}}\right) \quad \text{where} \tag{6}$$

$$B = \frac{q\mu N_C A}{d}\exp\left(\frac{-q\phi_\mathrm{T}}{k_\mathrm{B}T}\right),\ C = \frac{\sqrt{\frac{q^3}{\pi\varepsilon_0\varepsilon d}}}{k_\mathrm{B}T}. \tag{7}$$

In order to cover the whole range of the I-V-characteristic, we design our model using two exponential terms - one describing the on-switching (set) at negative applied voltages and one for off-switching (reset) under positive applied voltages. Using (6) the nonlinear memristor conductance is designed as:

$$G_\mathrm{m}(x, V_\mathrm{m}) = B_\mathrm{reset}\exp\left(C_\mathrm{reset}\,\mathrm{sign}(V_\mathrm{m})\sqrt{\frac{|V_\mathrm{m}|}{x}}\right) + B_\mathrm{set}\,x\,\exp\left(-C_\mathrm{set}\,\mathrm{sign}(V_\mathrm{m})\sqrt{|V_\mathrm{m}|}\right). \tag{8}$$

The state x dependency in (8) can be understood as a permittivity change for positive voltages (RESET) and a change in the barrier height of trapped charges for negative voltages (SET). The state in the second term of (8) emulates the decrease of the memristor conductivity during SET while decreasing the state as indicated in Fig. 5a with arrows. The fitted model parameters for (8) are given in Table I. For the state equation a generic approach with exponential dependency on current and voltage is analyzed (similar to [20]) and the fitting matches well with c_1, c_2, c_3 as follows:

$$\frac{\mathrm{d}x}{\mathrm{d}t} = c_1\left[\exp(c_2 I) - \exp(c_3|V|)\right] \cdot w(x), \tag{9}$$

where $w(x)$ is a window function limiting the state between 0 and 1. As window function $w(x) = 1 - (2x-1)^{20}$ from [21] is applied, but it hardly affects the state and is not limited to use other window functions. Equation (9) represents the extended generic memristor (3) when inserting the current function (4) and the state parameter from Table II. Since (4) is an implicit function, the extended generic memristor cannot be written in a closed form. The dynamic route map (DRM) of (9), illustrated in Fig. 4b, implies the non-volatile device behavior, i.e. no state change for zero input voltage also known as power-off plot (POP) (cf. dashed line in Fig. 4b). For positive voltages stable crossing points (see x_1, x_2, x_3 in Fig. 4b) can be observed, which means, that the input voltage highly influences the programmed state. Eq. (9) is mainly current dependent by the first term $\exp(c_2 I)$, while the second term $-\exp(c_3|V|)$ leads to a state decrease for small currents, which is in accordance with the measurement, cf. Fig. 4.

The complete MIIM model, defined with (4) and (8), is fitted in MATLAB solving the implicit current function to the measurement data set of $(\boldsymbol{I}, \boldsymbol{V})$ with

$$\min_{\substack{B_\mathrm{set}, B_\mathrm{reset}, C_\mathrm{set}, C_\mathrm{reset} \\ R_\mathrm{s}, R_\mathrm{p}, c_1, c_2, c_3, x_0}} \left\| \frac{\boldsymbol{V} - \boldsymbol{I}R_\mathrm{s}}{R_\mathrm{p}}\left(R_\mathrm{p}\,G_\mathrm{m}(x, \boldsymbol{V}, \boldsymbol{I}) + 1\right) - \boldsymbol{I}\right\|_2^2 \tag{10}$$

by solving the state equation (9) for every time step with

$$x = x_0 + c_1 \int \left[\exp(c_2 I) - \exp(c_3|V|)\right] \cdot w(x)\,\mathrm{d}t. \tag{11}$$

TABLE I: Conduction model parameter

B_set	B_reset	C_set	C_reset	R_p	R_s
7.5 nS	10.7 nS	8.7 $\mathrm{V}^{-1/2}$	4.5 $\mathrm{V}^{-1/2}$	11.86 MΩ	266 Ω

TABLE II: State model parameter

c_1	c_2	c_3	x_0
0.011	5.54	0.25	0.34

Post-print version of the article: R. Schroedter, E. Mgeladze, M. Herzig, A. Ascoli, S. Slesazeck, T. Mikolajick, R. Tetzlaff, "Physics-based modeling of a bi-layer Al2O3/Nb2O5 analog memristive device", *Proc. of the IEEE International Symposium on Circuits and Systems (ISCAS), 2022, Austin, TX, USA*, 2022. DOI: 10.1109/ISCAS48785.2022.9937966

For further information contact: richard.schroedter[at]tu-dresden.de, ORCID: 0000-0003-3259-4571

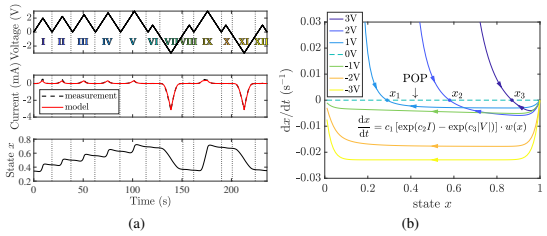

(a) (b)

Fig. 4: State model: (a) time evolution of voltage, current and state for gradual RESET followed by a full SET, RESET and SET (activation omitted); (b) Dynamic route map (DRM) of state evolution (9) for positive/negative input voltages (upper/lower) showing stable states for positive input voltage at x_1=0.29, x_2=0.58, x_3=0.87 for $[1, 2, 3]V$

The time plots in Fig. 4a prove a distinct state change of the model for the SET and RESET of the device. The proposed compact model (4) and (9) shows high agreement with the experimental data ($R^2 = 0.996$) as demonstrated in Fig. 5a.

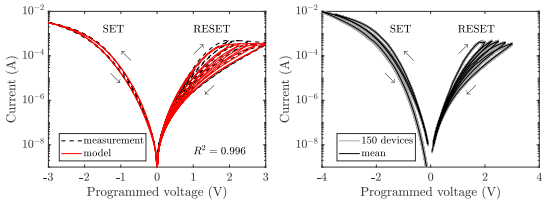

(a) (b)

Fig. 5: Model verification: (a) I-V measurement (data from Fig. 1a) and model with $R^2 = 0.996$; (b) I-V measurements for 150 different devices (gray lines is data of 150 devices overlapped, black line is the mean of all curves). Arrows show the direction of the I-V plots for increasing time.

In addition to the graphical analysis, the I-V curves at different ambient temperatures in Fig. 6a are measured, which confirm a clear temperature dependency as expected for Poole-Frenkel conduction, cf. (5). The trap energy level Φ_T is determined from the slope of the Arrhenius plot to vary between 0.31 and 0.48 eV, see Fig. 6b, indicating a thermal release of the trapped charges and the activation energy increases for higher voltages.

VI. Discussion

Modeling of memristive devices can be a difficult task, since the interaction and impact of multiple physical mechanisms that occur in these devices cannot easily be separated from each other. Therefore, this paper proposes a graphical analysis based on the exponential derivative γ revealing the equivalent circuit. Then linear fitting in different plots is applied by assuming possible conduction mechanisms, like ohmic with $\ln(J)$ vs. $\ln(E)$ and Poole-Frenkel with $\ln(J/E)$ vs. $\sqrt{E}$ in this case. From this linear fitting, the free parameter, e.g. parallel resistance R_p and permittivity ε, are considered as to be state dependent. Several approaches for the differential

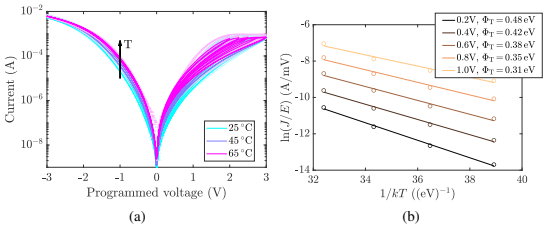

(a) (b)

Fig. 6: Temperature measurements: (a) I-V measurements varying ambient temperatures at 25, 45 and 65 °C (data as points and lines are fitted using the model); (b) Arrhenius plot for voltages up to 1 V (during RESET in section IX cf. Fig. 4a)

state equation have been tested, e.g. exponential terms for current, voltage, state for set and reset individually, resulting in the presented state function (9) with high agreement to the measurement. However, the current still tends to be smaller than the measurement for high voltages, cf. Fig. 5a, which can be due to the fact, that the proposed model does not fit negative γ values like reset 6 in Fig. 1b. One remarkable behavior of the presented device is the full reset 6 in Fig. 1a, which starts as reset 1 but returns in overlap with reset 5. A strong voltage dependency is assumed and covered with the presented model, which is confirmed by the DRM showing stable state for the reset.

The measurements are from a device with 50 µm diameter size of the contact electrode. In any case, scalability by about 3 orders of magnitude would be beneficial for high integration in a crossbar array. More than 150 different devices have been measured, showing the similar I-V curve behavior, see Fig. 5b. Consequently, a small device-to-device variability is assumed, but more analysis needs to be done in future for full confidence.

This paper demonstrates a physics-based compact model for an analog bi-layer Al_2O_3/Nb_2O_5 memristive device, which can be applied for simulation and optimization of the integration to memristive crossbar arrays for neuromorphic computing application.

VII. Conclusion

Based on quasi-static I-V measurements of a memristive bi-layer Al_2O_3/Nb_2O_5 stack, a physics-based model is derived for application in neuromorphic computing. It was shown, that analog multi-level switching at high resistances without electroforming is performed, which is favorable for crossbar operations with low energy consumption. Graphical analysis with the exponential derivative and considering ohmic and Poole-Frenkel conduction mechanisms lead to a compact model, represented by an algebraic differential equation. The model was fitted to experimental I-V data with high agreement ($R^2 = 0.996$) mapping the overall device behavior. Temperature measurements confirm the imposed Poole-Frenkel emission, but further analysis including pulse input measurements and considering also the memcapacitance behavior are part of future research.

Post-print version of the article: R. Schroedter, E. Mgeladze, M. Herzig, A. Ascoli, S. Slesazeck, T. Mikolajick, R. Tetzlaff, "Physics-based modeling of a bi-layer Al2O3/Nb2O5 analog memristive device", *Proc. of the IEEE International Symposium on Circuits and Systems (ISCAS), 2022, Austin, TX, USA*, 2022. DOI: 10.1109/ISCAS48785.2022.9937966

For further information contact: richard.schroedter[at]tu-dresden.de, ORCID: 0000-0003-3259-4571

References

[1] Q. Xia and J. J. Yang, "Memristive crossbar arrays for brain-inspired computing," *Nature Materials*, vol. 18, no. 4, pp. 309–323, Apr. 2019. [Online]. Available: https://doi.org/10.1038/s41563-019-0291-x

[2] R. Tetzlaff, Ed., *Memristors and Memristive Systems*. New York, NY: Springer New York, 2014. [Online]. Available: https://doi.org/10.1007/978-1-4614-9068-5

[3] F. M. Bayat, M. Prezioso, B. Chakrabarti, H. Nili, I. Kataeva, and D. Strukov, "Implementation of multilayer perceptron network with highly uniform passive memristive crossbar circuits," *Nature Communications*, vol. 9, no. 1, p. 2331, Jun. 2018. [Online]. Available: https://doi.org/10.1038/s41467-018-04482-4

[4] F. Cai, J. M. Correll, S. H. Lee, Y. Lim, V. Bothra, Z. Zhang, M. P. Flynn, and W. D. Lu, "A fully integrated reprogrammable memristor–CMOS system for efficient multiply–accumulate operations," *Nature Electronics*, vol. 2, no. 7, pp. 290–299, Jul. 2019. [Online]. Available: https://doi.org/10.1038/s41928-019-0270-x

[5] R. Waser, R. Dittmann, G. Staikov, and K. Szot, "Redox-Based Resistive Switching Memories – Nanoionic Mechanisms, Prospects, and Challenges," *Advanced Materials*, vol. 21, no. 25-26, pp. 2632–2663, 2009. [Online]. Available: https://doi.org/10.1002/adma.200900375

[6] M. Hansen, M. Ziegler, L. Kolberg, R. Soni, S. Dirkmann, T. Mussenbrock, and H. Kohlstedt, "A double barrier memristive device," *Scientific Reports*, vol. 5, no. 1, p. 13753, Nov. 2015. [Online]. Available: https://doi.org/10.1038/srep13753

[7] N. Alimardani, J. M. McGlone, J. F. Wager, and J. F. Conley, "Conduction processes in metal–insulator–metal diodes with Ta_2O_5 and Nb_2O_5 insulators deposited by atomic layer deposition," *Journal of Vacuum Science & Technology A: Vacuum, Surfaces, and Films*, vol. 32, no. 1, p. 01A122, Jan. 2014. [Online]. Available: https://doi.org/10.1116/1.4843555

[8] I. N. Noureddine, N. Sedghi, I. Z. Mitrovic, and S. Hall, "Barrier tuning of atomic layer deposited Ta2O5 and Al2O3 in double dielectric diodes," *J. Vac. Sci. Technol. B*, vol. 35, no. 1, p. 6, 2017. [Online]. Available: https://doi.org/10.1116/1.4974219

[9] I. Z. Mitrovic, A. D. Weerakkody, N. Sedghi, J. F. Ralph, S. Hall, V. R. Dhanak, Z. Luo, and S. Beeby, "Controlled modification of resonant tunneling in metal-insulator-insulator-metal structures," *Applied Physics Letters*, vol. 112, no. 1, p. 012902, Jan. 2018. [Online]. Available: https://doi.org/10.1063/1.4999258

[10] H. Mähne, H. Wylezich, F. Hanzig, S. Slesazeck, D. Rafaja, and T. Mikolajick, "Analog resistive switching behavior of Al/Nb2O5/Al device," *Semiconductor Science and Technology*, vol. 29, no. 10, p. 104002, Sep. 2014. [Online]. Available: https://doi.org/10.1088/0268-1242/29/10/104002

[11] H. Wylezich, E. Reinhardt, S. Slesazeck, and T. Mikolajick, "Integration of niobium oxide-based resistive switching cells with different select properties into nanostructured cross-bar arrays," *Semiconductor Science and Technology*, vol. 30, no. 11, p. 115014, Oct. 2015. [Online]. Available: https://doi.org/10.1088/0268-1242/30/11/115014

[12] S. Slesazeck, H. Wylezich, and T. Mikolajick, "Analog memristive and memcapacitive properties of Ti / AI2O3 / Nb2O5 / Ti resistive switches," in *2017 IEEE 8th Latin American Symposium on Circuits Systems (LASCAS)*, Feb. 2017, pp. 1–4. [Online]. Available: https://doi.org/10.1109/LASCAS.2017.7948106

[13] A. Ascoli, A. S. Demirkol, R. Tetzlaff, S. Slesazeck, T. Mikolajick, and L. O. Chua, "On Local Activity and Edge of Chaos in a NaMLab Memristor," *Frontiers in Neuroscience*, vol. 15, 2021. [Online]. Available: https://doi.org/10.3389/fnins.2021.651452

[14] H. Wylezich, "Integration und Charakterisierung resistiv schaltbarer Speichermatrizen," Dissertation, Technische Universität Dresden, 2016, research at NaMLab.

[15] C. Acha, "Graphical analysis of current-voltage characteristics in memristive interfaces," *Journal of Applied Physics*, vol. 121, no. 13, p. 134502, Apr. 2017. [Online]. Available: https://doi.org/10.1063/1.4979723

[16] R. Tetzlaff, A. Ascoli, I. Messaris, and L. O. Chua, "Theoretical foundations of memristor cellular nonlinear networks: Memcomputing with bistable-like memristors," *IEEE Transactions on Circuits and Systems I: Regular Papers*, vol. 67, no. 2, pp. 502 – 515, 2019. [Online]. Available: https://doi.org/10.1109/TCSI.2019.2940909

[17] Z. Wang, S. Kumar, Y. Nishi, and H.-S. P. Wong, "Transient dynamics of NbOx threshold switches explained by Poole-Frenkel based thermal feedback mechanism," *Applied Physics Letters*, vol. 112, no. 19, p. 193503, May 2018. [Online]. Available: https://doi.org/10.1063/1.5027152

[18] H. Spahr, S. Montzka, J. Reinker, F. Hirschberg, W. Kowalsky, and H.-H. Johannes, "Conduction mechanisms in thin atomic layer deposited Al2O3 layers," *Journal of Applied Physics*, vol. 114, no. 18, p. 183714, Nov. 2013. [Online]. Available: https://doi.org/10.1063/1.4829910

[19] H. García, H. Castán, E. Perez, S. Dueñas, L. Bailón, T. Blanquart, J. Niinistö, K. Kukli, M. Ritala, and M. Leskelä, "Influence of growth and annealing temperatures on the electrical properties of Nb_2O_5 -based MIM capacitors," *Semiconductor Science and Technology*, vol. 28, no. 5, p. 055005, May 2013. [Online]. Available: https://doi.org/10.1088/0268-1242/28/5/055005

[20] X. Guan, S. Yu, and H.-S. P. Wong, "A SPICE Compact Model of Metal Oxide Resistive Switching Memory With Variations," *IEEE Electron Device Letters*, vol. 33, no. 10, pp. 1405–1407, Oct. 2012. [Online]. Available: https://doi.org/10.1109/LED.2012.2210856

[21] Y. N. Joglekar and S. J. Wolf, "The elusive memristor: Properties of basic electrical circuits," *European Journal of Physics*, vol. 30, no. 4, pp. 661–675, May 2009. [Online]. Available: https://doi.org/10.1088/0143-0807/30/4/001

Post-print version of the article: R. Schroedter, E. Mgeladze, M. Herzig, A. Ascoli, S. Slesazeck, T. Mikolajick, R. Tetzlaff, "Physics-based modeling of a bi-layer Al2O3/Nb2O5 analog memristive device", *Proc. of the IEEE International Symposium on Circuits and Systems (ISCAS), 2022, Austin, TX, USA*, 2022. DOI: 10.1109/ISCAS48785.2022.9937966

For further information contact: richard.schroedter[at]tu-dresden.de, ORCID: 0000-0003-3259-4571